Cell Volume Measured by Total Internal Reflection Microfluorimetry: Application to Water and Solute Transport in Cells Transfected with Water Channel Homologs

Javier Farinas,‡ Veronika Simanek,* and A. S. Verkman*‡
*Departments of Medicine and Physiology, Cardiovascular Research Institute, and ‡Program in Biophysics, University of California, San Francisco, California 94143-0521 USA

ABSTRACT Total internal reflection (TIR) microfluorimetry was established as a method to measure continuously the volume of adherent cells and applied to measure membrane permeabilities in cells transfected with water channel homologs. Cytosol was labeled with the membrane-impermeant fluorophore calcein. Fluorescence was excited by the TIR evanescent field in a thin section of cytosol (~150 nm) adjacent to the cell-substrate interface. Because cytosolic fluorophore number per cell remains constant, the TIR fluorescence signal should be inversely related to cell volume. For small volume changes in Sf-9 and LLC-PK1 cells, relative TIR fluorescence was nearly equal to inverse relative cell volume; deviations from the ideal were modeled theoretically. To measure plasma membrane osmotic water permeability, P_f, the time course of osmotically induced cell volume change was inferred from the TIR fluorescence signal. LLC-PK1 cells expressing the CHIP28 water channel had an $HgCl_2$-sensitive, threefold increase in P_f compared to nontransfected cells (P_f = 0.0043 cm/s at 10°C). Solute permeability was measured from the TIR fluorescence time course in response to solute gradients. Glycerol permeability in Sf-9 cells expressing the water channel homolog GLIP was $(1.3 \pm 0.2) \times 10^{-5}$ cm/s (22°C), greater than that of $(0.36 \pm 0.04) \times 10^{-5}$ cm/s ($n = 4$, $p < 0.05$) for control cells, indicating functional expression of GLIP. Water and urea permeabilities were similar in GLIP-expressing and control cells. The TIR method should be applicable to the study of water and solute permeabilities and cell volume regulation in cells of arbitrary shape and size.

INTRODUCTION

The measurement of volume in cultured cells has a number of biological applications, including the analysis of cell volume regulatory mechanisms (Montrose-Rafizadeh and Guggino, 1990), and the determination of plasma membrane water and solute permeabilities (Verkman, 1993). Stopped-flow light scattering (Van Hoek and Verkman, 1992) and fluorescence quenching (Verkman et al., 1988) methods have been applied to measure volume changes in suspensions of small biomembrane vesicles and proteoliposomes reconstituted with transporting proteins. However, stopped-flow methods are in general not suitable to study living cells because the majority of light scattered from intact cells arises from intracellular structures which do not participate in an osmotic response. In addition, the suspension of cells grown on solid supports disrupts cell polarity and morphology.

Several approaches have been applied to estimate cell volume changes in adherent cells. A light scattering method was developed to measure osmotic volume changes in J774 macrophages grown on glass coverslips based on the cell volume-dependence of light scattered by the cell surface (Fischbarg et al., 1989; Echevarria and Verkman, 1992). This approach yielded an adequate volume-dependent signal for hemispherical J774 cells that formed confluent monolayers, but did not produce measurable signals in our laboratory for other types of cells. Muallem et al. (1992) reported a fluorescence microscopy method to follow cell volume in which the aqueous phase of cytosol was labeled with a fluorescent indicator and cell fluorescence was monitored with a high magnification, high numerical aperture objective. The partial confocality achieved in this configuration confers a weak dependence of detected fluorescence on fluorophore concentration and thus cell volume. However, this method produces variable small signals which depend strongly on cell morphology and the details of the optical configuration. Kao et al. (1994) recently introduced a refinement of the single particle tracking method to measure the vertical position of a fluorescent bead immobilized at the cell surface. Cell swelling and shrinking were followed from the time course of bead rising and falling. Single particle tracking is useful to study effects of putative agonists and antagonists on volume changes in single cells; however, because of uncertainties in bead location and cell morphology, quantitative data on cell volume changes cannot be obtained. Finally, Strange and Spring (1987) have utilized image analysis methods to determine the volume of cells in kidney tubule epithelia in response to osmotic gradients. The use of imaging methods and confocal optics could in principal provide a quantitative approach to study volume changes in adherent cells, however the extensive computational requirements and the limited spatial resolution of conventional light microscopy restrict practical applications.

The purpose of this study was to develop a quantitative method to continuously measure the relative volume of adherent cultured cells. As shown schematically in Fig. 1 *A*, cytosol was labeled with a membrane-impermeant, aqueous-phase fluorophore. Total internal reflection (TIR) microfluorimetry was utilized to quantify the fluorescence excited by

Received for publication 3 November 1994 and in final form 25 January 1995.

Address reprint requests to Javier Farinas, 1246 Health Sciences East Tower, University of California, San Francisco, CA 94143-0521. Tel.: 415-476-8530; Fax: 415-665-3847; E-mail: javier@itsa.ucsf.edu.

© 1995 by the Biophysical Society

0006-3495/95/04/1613/08 $2.00

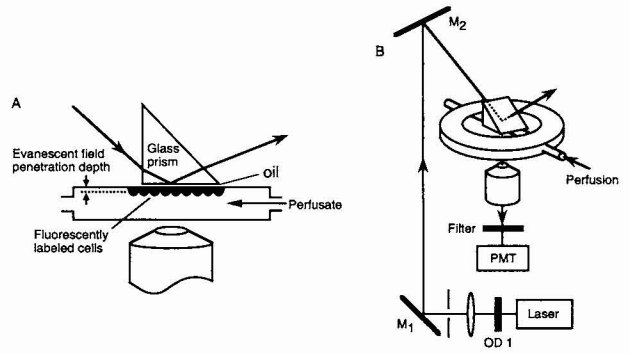

FIGURE 1 Schematic drawing of the TIR microfluorimetry apparatus. Fluorescence is excited in a section of fluorescently labeled cytosol adjacent to a glass-aqueous interface and collected by an objective lens. See Materials and Methods for details.

the evanescent field in a very thin layer of cytosol (~150 nm) adjacent to the glass-aqueous interface. Because the total number of fluorophores in cytosol is constant, fluorophore concentration, and thus emitted fluorescence, is predicted to be inversely related to relative cell volume. The TIR method provided a simple and general approach to measure accurately and in real time the relative volume of adherent cells of arbitrary size and shape. This report validates the TIR method for cell volume measurements, and applies this method to measure water and solute permeabilities in cells transfected with recently cloned water channels.

MATERIALS AND METHODS

Cell culture

Cell monolayers were cultured on 18 mm diameter, round glass coverslips. Sf-9 insect cells (American Type Culture Collection No. CRL 1711, Rockville, MD) were grown at 28°C in SFM-II serum-free medium. The coding sequences for water channel homologs WCH-CD (Fushimi et al., 1993) and GLIP (Ma et al., 1994; Frigeri et al., 1995) were subcloned into plasmid pBlueBac III (Invitrogen, San Diego, CA) and cotransfected into Sf-9 cell monolayers with wild-type, *Autographa californica* nuclear polyhedrosis viral DNA using cationic liposomes. Purified recombinant virus was isolated by serial plaque assays and propagated to high titer (~10^8 plaque forming units/ml) by standard methods (O'Reilly et al., 1994). Protein expression and plasma membrane localization were confirmed by immunofluorescence and immunoblot with peptide-derived polyclonal antibodies (data not shown). For water and solute transport studies, Sf-9 cell monolayers were infected with wild-type, GLIP-recombinant or WCH-CD-recombinant baculovirus at a multiplicity of infection of 3–5. Permeabilities were measured at 2 days post-infection.

Untransfected and CHIP28-transfected LLC-PK1 pig kidney epithelial cells (American Type Culture Collection No. CL 101) were provided by Dennis Brown and grown in M199 medium supplemented with 10% fetal calf serum, 100 U/ml penicillin and 100 mg/ml streptomycin. Cells were maintained at 37°C in a 95% air/5% CO_2 atmosphere.

Total internal reflection microfluorimetry

Relative cell volume was measured from the TIR fluorescence of the cell-entrapped, fluorescent dye calcein-AM. Fig. 1 *B* shows a schematic of the apparatus. The perfusion chamber containing the cultured cells was mounted on the stage of a Nikon Diaphot inverted microscope. A 442-nm laser beam from a 4230NB HeCd laser (35 mW, Liconix, Santa Clara, CA) was attenuated 10-fold by a neutral density filter, focused with a biconvex lens (40 cm focal length), and directed through a 1 mm diameter circular aperture. Beam incidence angle was adjusted from the vertical position of mirror M_2. A right-triangular, glass prism (7 mm edge length, refractive index n = 1.517) was optically coupled to the cell-free surface of the cover glass by type DF immersion oil (n = 1.515). Maximum beam intensity at the slide/water interface was 70 mW/cm^2. Emitted fluorescence was collected by a 25× dry objective (numerical aperture 0.35, working distance 16 mm, Leitz), filtered by a GG520 cut-on filter (Schott Glass, Duryea, PA) and detected by a type B2/RFI photomultiplier (Thorn EMI, Middlesex, England). Photomultiplier current was amplified (model 110, Pacific Instruments) and digitized by a 12-bit analog-to-digital converter interfaced to a 486 PC computer. Data were generally collected at a rate of 5 Hz.

A stainless steel cell perfusion chamber containing a 1.5 × 2.5 × 14 mm ($w \times h \times l$) channel was constructed. The top of the perfusion chamber was bounded by the cover glass containing the cultured cells (facing downward) and the bottom of the chamber was bounded by a blank coverslip. Perfusion solutions were gravity fed (flow generally 5–12 ml/min) and switched by a Hamilton four-way valve. Perfusate temperature was maintained by an in-line metallic cooling coil (stainless steel, length 40 mm, inner diameter 1 mm, outer diameter 1.2 mm) submerged in a water bath just proximal to the perfusion chamber. Effluent temperature was monitored by an in-line thermistor.

Cell imaging

A custom built upright fluorescence microscope and perfusion chamber were used to image cells at high magnification (Bicknese et al., 1994). Cells grown on glass coverslips were either loaded with calcein or placed in solutions containing 1 mg/ml of the membrane impermeable dye FITC-dextran (4 kDa). The cells were illuminated from below with a 488 nm Ar laser beam and imaged with either a 100× water immersion objective (numerical aperture 1.2, working distance 0.17 mm, Leitz) or a 25× dry objective (numerical aperture 0.35, working distance 16 mm, Leitz). Emitted fluorescence passed through a 515-nm cut-on filter and was detected by a 14-bit cooled CCD camera (Photometrics Ltd., Tucson, AZ). The laser beam could be rapidly switched between supercritical and subcritical angles to produce TIR or trans-illuminated images, respectively. Images were acquired and analyzed using PMIS software (Photometrics).

Cell surface-to-volume ratios were calculated from serial confocal images of calcein-loaded cells using a K2-Bio Nipkow wheel confocal microscope (Technical Instruments, San Francisco, CA). Fluorescence was excited and measured with a fluorescein-filter set, a PlanApo 60× oil immersion objective (numerical aperture 1.4, Nikon, Melville, NY) and a cooled CCD camera. Image z-resolution was ~0.9 μm. Cell images were recorded at 4.5-μm intervals starting 2.25 μm above the glass substrate. Cell volume was calculated by summing the volume of serial right cylindrical sections. Cell surface area was calculated by a reconstruction procedure: the boundary of each cell slice was defined by points spaced at 30-degree intervals. A surface was reconstructed by joining neighboring points to form a series of triangular faces. Total surface area was calculated by summing the areas of each triangular face and the top and bottom surfaces.

Permeability measurements

Cells were used before confluence. Before microscopy measurements, cells were washed with PBS (in mM: 137 NaCl, 0.9 $CaCl_2$, 0.49 $MgCl_2$, 2.7 KCl, 1.5 KH_2PO_4, 8.1 Na_2HPO_4, pH 7.4) and incubated for 20 min with PBS containing 10 μM calcein-AM (Molecular Probes, Eugene, OR) added from a 10 mM stock solution in DMSO. Water permeability was measured from the time course of TIR fluorescence in response to osmotic gradients. Cells were initially perfused with PBS and then subjected to specified osmotic gradients using solutions containing PBS diluted with distilled water (hypotonic) or containing NaCl (hypertonic). The time course of TIR fluorescence for each experiment was fitted with a single exponential function, $F(t) = \alpha + \beta \exp(-t/\tau)$.

The osmotic water permeability, P_f, was calculated from the exponential time constant, τ, by using the equation describing net volume flow across a semipermeable membrane:

$$d(V/V_o)/dt = -P_f V_w (A/V)_o \Delta\phi_o \quad (1)$$

where $d(V/V_o)/dt$ is the initial rate of relative cell volume change, $(A/V)_o$ is the initial cell surface-to-volume ratio, V_w is the partial molar volume of water (18 cm^3/mole) and $\Delta\phi_o$ is the initial osmotic gradient (outside-inside).

To solve for P_f, V/V_o must be related to the measured relative fluorescence F/F_o. For small osmotic gradients (see Fig. 3 *A*), F/F_o is found empirically to relate to relative osmolality, ϕ/ϕ_o, by the equation

$$F/F_o = \chi + \gamma(\phi/\phi_o) \quad (2)$$

where γ is the slope of the relative fluorescence versus relative osmolality calibration curve at a relative osmolality of unity. Cell volume is related to osmolality by the equation (see Appendix)

$$(V_o - b)/(V - b) = \phi/\phi_o \quad (3)$$

where b/V_o is the fractional content of cell solids. Combining Eqs. 1–3,

$$P_f = [d(F/F_o)/dt](1 - b/V_o)[\gamma(A/V)_o V_w \Delta\phi_o]^{-1} \quad (4)$$

The value of γ is calculated for each time course from the exponential fit by recognizing that $\gamma = \Delta(F/F_o)/\Delta(\phi/\phi_o) = (-\beta\phi_o)/([\alpha + \beta][\Delta\phi_o])$. Because the exponential time constant, τ, is equal to $-\beta/([\alpha + \beta][d(F/F_o)/dt])$ and assuming that $b = 0$, Eq. 4 simplifies to

$$P_f = [\tau(A/V)_o V_w \phi_o]^{-1} \quad (5)$$

Plasma membrane solute permeability was measured from the time course of cell TIR fluorescence in response to solute gradients. In response to an inwardly directed gradient of a permeant solute, cell volume initially decreases by water efflux and then increases due to solute (and water) influx. The solute permeability coefficient, P_s, can be related to the rate of cell swelling using the expression for net solute flux across a semipermeable membrane in response to a solute gradient $(S_{out} - S_{in})$,

$$d(V/V_o)/dt = (A/V)_o P_s(S_{out} - S_{in})/\phi_o \quad (6)$$

Applying the assumptions used for derivation of Eq. 5, and assuming that solute movement is much slower than osmotic water movement ($P_s \ll P_f$) and that the solute reflection coefficient is near unity, it follows that

$$P_s = -(d(F/F_o)/dt)[(F_o - F_\infty)(A/V)_o(1 - \{S_o - S_{in}\}/\phi_o)]^{-1} \quad (7)$$

where $F_o - F_\infty$ is the amplitude of the fluorescence decay and $d(F/F_o)/dt$ is the initial slope of the fluorescence time course during the phase of solute entry, determined from an empirical fit to the data.

RESULTS

Fig. 2 shows the fluorescence signal from monolayers of uninfected Sf-9 cells perfused with solutions of various osmolalities. Cell cytoplasm was stained with calcein, a fluid-phase pH-insensitive fluorophore. As expected, excitation of calcein fluorescence by trans-illumination (subcritical illumination angle, 30°) produced a signal which was insensitive to perfusate osmolality (and thus cell volume) (left portion of figure). In contrast, the signal produced by TIR illumination was strongly dependent upon perfusate osmolality; the signal decreased upon perfusion with hypotonic solution as a consequence of osmotic water influx, cell swelling, and decreased cytoplasmic calcein concentration. Similarly, the TIR signal increased upon perfusion with a hypertonic solution. Photobleaching caused a significant decline in fluorescence baseline with trans- but not TIR illumination.

The TIR fluorescence signal is, in principle, sensitive to changes in fluorophore concentration and to the penetration depth of the evanescent field. The penetration depth depends upon the refractive index of the aqueous phase, as well as upon excitation wavelength, refractive index of the glass prism, and laser beam illumination angle (Hecht, 1987). To confirm that the

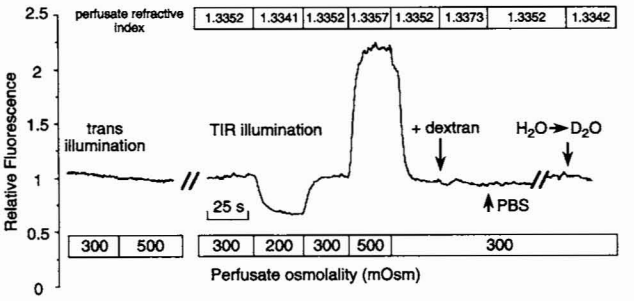

FIGURE 2 Relative fluorescence from Sf-9 cells containing cytoplasmic calcein. Fluorescence was excited with trans-illumination and then by TIR illumination. Perfusate osmolality is shown at the bottom. The arrow labeled "+ dextran" indicates addition of 3% dextran (w/w) (MW = 40,000) to an isosmolar solution. The arrow labeled "$H_2O \rightarrow D_2O$" indicates the switch to an isosmolar solution containing 20% D_2O. Perfusate refractive index is shown at the top.

relative TIR fluorescence signal was dependent on perfusate osmolality and not on perfusate or cytoplasmic refractive indices, perfusate and cytoplasmic refractive indices were changed while keeping osmolality constant. There was no significant change in TIR fluorescence upon addition of 3% (w/w) dextran (Fig. 2, first arrow), which increased perfusate refractive index appreciably without altering perfusate osmolality. The influence of cytoplasmic refractive index on the TIR fluorescence signal was investigated by replacing the perfusate with an isosmolar solution containing 20% D_2O. Because equilibration of D_2O across the cell plasma membrane occurs rapidly and does not alter cell volume, changes in TIR fluorescence must result from refractive index effects. Fig. 2 (portion of curve at the right) shows that switching from PBS ($n = 1.3352$) to PBS containing 20% D_2O ($n = 1.3342$) did not change the fluorescence signal appreciably. These results indicate that the TIR fluorescence signal is sensitive to changes in cell volume and not to changes in perfusate or intracellular refractive index. Further, the relative change in TIR fluorescence in response to a given osmotic gradient did not depend on the angle of incidence of the laser beam (and thus on the evanescent field probe depth) over the range of 72–77° (critical angle 62°). Subsequent experiments were conducted with an illumination angle of 72°.

To determine the relationship between TIR fluorescence and cell volume, TIR fluorescence was measured in Sf-9 and LLC-PK1 cells for a series of perfusate osmolalities (Fig. 3 *A*). Theoretically, relative TIR fluorescence should be equal to relative solution osmolality (*solid line*) if the cells function as perfect osmometers (see below). For small changes in osmolality, the TIR signals from the calcein-loaded cells were close to the theoretical line. However, significant deviations occurred for greater changes in osmolality, most pronounced in the LLC-PK1 cells at high osmolality.

Several possible explanations for the non-ideal dependence of TIR fluorescence signal on relative osmolality were evaluated theoretically (see Appendix). Fig. 3 *B* shows the predictions of four simple models. Curve *a* is the linear prediction for a perfect osmometer in which the TIR evanescent field depth is much smaller than cell height and all intra-

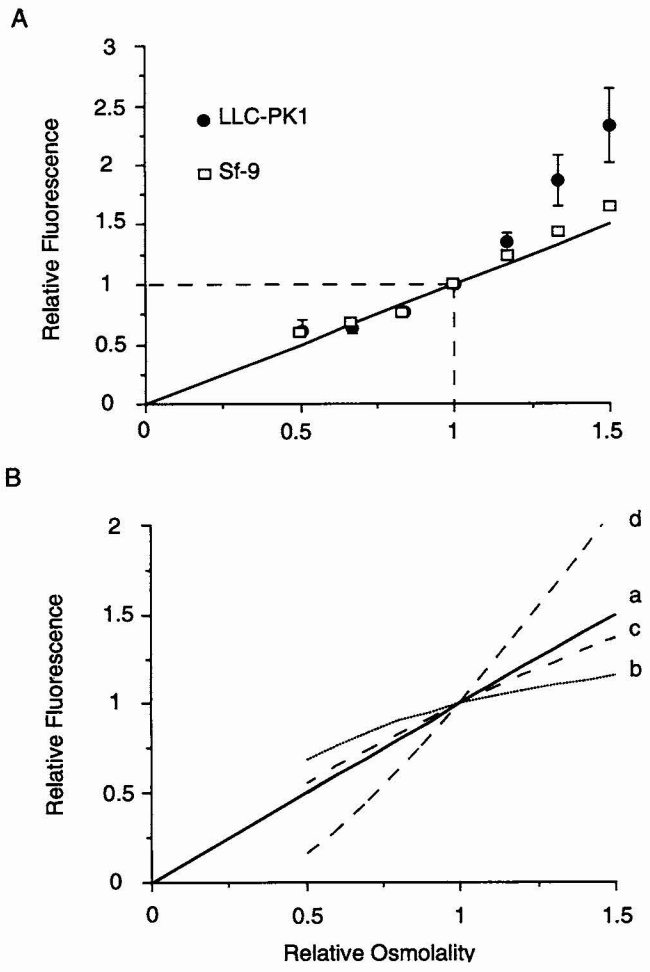

FIGURE 3 Dependence of relative TIR fluorescence on perfusate osmolality. (*A*) Relative TIR fluorescence of Sf-9 cells (□) and LLC-PK1 cells (●) as a function of relative perfusate osmolality. Data are plotted as the mean ± SE of 8–12 observations. The predicted behavior of a perfect osmometer is shown as a solid line for comparison. (*B*) Results of four models are shown: *a*) ideal osmometer, Eq. A-4; *b*) the effect of a thick evanescent probe depth, Eq. A-5, $\beta V_o = 0.5$; *c*) cells with osmotically inactive volume, Eq. A-6, $b = 0.2$; and *d*) the effect of cell shape changes, Eq. A-7, $\rho_o = 1.13$, $\sigma_o = 0.205$. See Appendix and text for details.

cellular volume is osmotically active. Curve *b* was generated by assuming perfect osmometric behavior but with a larger evanescent field probe depth (exponential depth constant to cell height ratio = 2), resulting in illumination of a thicker cell section. The downward concavity of the relative fluorescence versus osmolality curve is opposite to that observed experimentally. The evanescent field penetration for the experiments in Fig. 3 *A* was ~150 nm, much less than the average cell height of ~10 μm; for this very small penetration/height ratio, the model predicted no noticeable curvature (not shown). Curve *c* was generated for cells having non-zero osmotically inactive volume (20% of initial cell volume) arising from cell solids including proteins and lipids (Kao et al., 1993). The smaller slope of curve *c* compared to that of curve *a* results from progressive exclusion of fluorophore (by dye-excluding particulates) from the evanescent field as cell volume decreases. It is predicted that at high osmolality, curve *c* asymptotically approaches a maximum relative fluorescence equal to the reciprocal of the fraction of osmotically inactive volume. Experimentally, the relative fluorescence measured in Sf-9 cells for a large relative osmolality of 20 was >12, indicating little effect of cell solids on curve shape in our experiments. The absence of an influence of cell solids is probably due to a sieving effect of the membrane cytoskeleton which results in the relative exclusion of cell solids from the evanescent field (Luby-Phelps et al., 1986).

Thus, neither penetration depth-cell height considerations nor osmotically inactive volume can account for the greater than unity slope of the relative fluorescence versus relative osmolality data in Fig. 3 *A*. For relative osmolality >1, the experimental results suggest that cell shape is modified such that more fluorophores appear in the evanescent field than are predicted by the simple concentrating effect of cell shrinkage. Curve *d* was computed from a simple geometric model in which changes in cell shape accompany volume change. Although the qualitative agreement between curve *d* and the experimental data is consistent with but does not prove the cell shape model, it provides a possible explanation for the non-ideal osmotic behavior observed in LLC-PK1 cells. Other effects such as non-uniform dye distribution resulting from dye binding to intracellular structures could also explain the observed behavior but are difficult to model. For small relative osmolality values, the relative fluorescence is greater than predicted for simple osmometric behavior. This deviation is probably due to the inability of the cell to swell indefinitely because of mechanical restriction.

TIR fluorescence micrographs of Sf-9 cells perfused with 300, 150, and 500 mOsm solutions are shown in Fig. 4 *A*. As expected, TIR fluorescence signal intensity increases in hypertonic solution and decreases in hypotonic solution. There was little heterogeneity in TIR fluorescence signal over the cell, and the cell contact area remained fairly constant with changes in perfusate osmolality. To test the effect of osmolality on the cell-substrate contact distance, TIR fluorescence images of Sf-9 cells in solutions containing FITC-dextran were obtained. The ratio of TIR fluorescence in the area of cell contact to that between cells was determined as a semiquantitative measure of cell-substrate contact. As solution osmolality was increased from 300 to 500 mOsm, this ratio decreased from 0.63 to 0.56, indicating that the cell-substrate contact distance decreases as the cell shrinks. The small decrease in the cell-substrate contact distance at high osmolality caused more cytoplasm to be brought into the evanescent field. This effect is consistent with the cell shape change model described above (model *d*) and thus may account for the deviations seen in Fig. 3 *A*.

Representative serial confocal images of Sf-9 cells used for cell shape reconstruction are shown in Fig. 4 *B*. Fig. 4 *C* shows the reconstructed cell surfaces for an Sf-9 cell perfused with 300, 150, and 500 mOsm solutions. Note the elongated cell shape at low osmolality with little change in substrate contact area. The change in inverse relative volume of cells as a function of osmolality was calculated from the cell shape reconstructions. Compared to the volume at 300 mOsm, the inverse relative volume increased to 1.64 ± 0.09

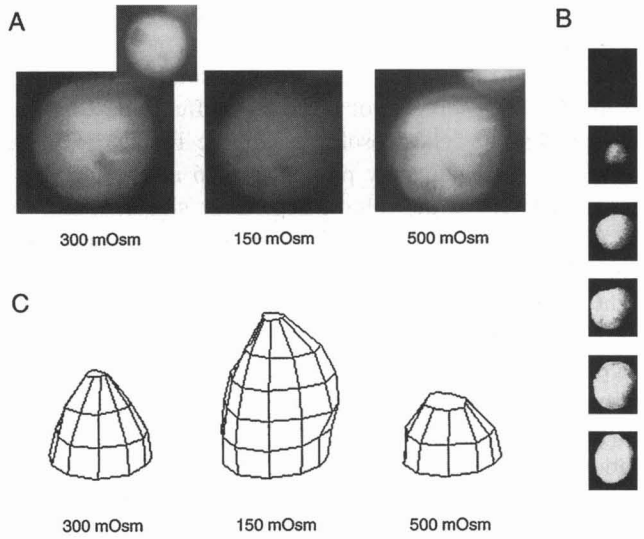

FIGURE 4 Photomicrographs of uninfected Sf-9 cells. (*A*) Calcein-loaded cells perfused in 300, 150, and 500 mOsm solutions and imaged at 100× with TIR illumination. The inset shows the corresponding trans-illuminated image at 300 mOsm. (*B*) Serial confocal cell images recorded at 4.5-μm intervals (bottom image is of the cell-substrate interface). (*C*) Representative cell surface reconstructions for a cell perfused with 300, 150, and 500 mOsm solutions.

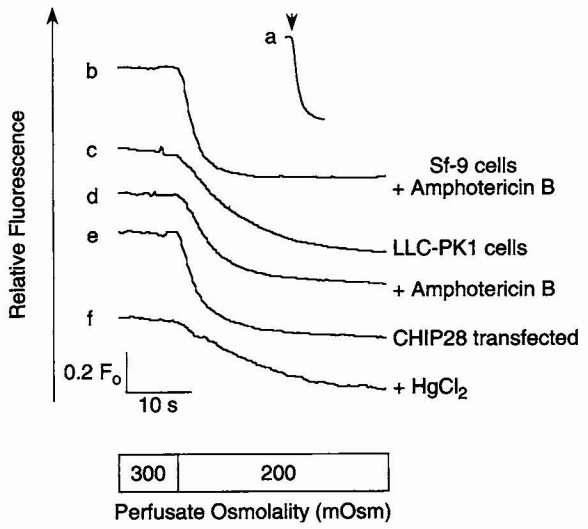

FIGURE 5 Measurement of cell plasma membrane osmotic water permeability. (*A*) Solution exchange time at a perfusion rate of 11 ml/min determined by exchange of 10 μM fluorescein with water. For *B–F*, cytoplasm was stained with calcein and the time course of TIR fluorescence was measured in response to a 100 mM outwardly directed osmotic gradient (200 mOsm perfusate) at 10°C. See text for averaged permeability values. (*B*) Rapid osmotic response for Sf-9 cells incubated with amphotericin B (50 μg/ml). (*C, D*) Non-transfected LLC-PK1 cells: control (*C*), and after incubation with amphotericin B (50 μg/ml) (*D*). (*E, F*) CHIP28-transfected LLC-PK1 cells: control (*E*), and after perfusion with 0.3 mM $HgCl_2$ (*F*).

at 500 mOsm and decreased to 0.63 ± 0.07 (SE, n = 8) at 150 mOsm. These calculated osmotic volume changes are consistent with the model predictions for perfect osmometric behavior. As described in Materials and Methods, such reconstructions were used to calculate surface-to-volume ratios of 4800 and 2500 cm^{-1} for LLC-PK1 and Sf-9 cells, respectively.

An application of the TIR fluorescence method to measure osmotic water permeability is presented in Fig. 5. To determine the perfusion exchange/instrument response time under the conditions of the cell experiments, a fluorescein-containing solution was replaced by water. The figure inset, *a*, shows the decrease in fluorescence with a response time of ~0.6 s. For the cell studies, the isosmolar (300 mOsm) perfusate was replaced by a hypotonic 200 mOsm perfusate to induce osmotic water influx at 10°C. Curve *b* shows a very fast osmotic response in Sf-9 cells preincubated with the artificial pore-forming agent amphotericin B (50 μg/ml). The average time constant for the TIR fluorescence response was 2.6 s. Given the perfusion exchange/instrument response time, this represents the fastest resolvable rate of volume change. Representative curves for LLC-PK1 cells (*c*), LLC-PK1 cells preincubated with 50 μg/ml Amphotericin B (*d*) and CHIP28-transfected LLC-PK1 cells (*e*) give averaged exponential time constants of 10 ± 1, 4.9 ± 0.3, and 3.3 ± 0.3 s (mean ± SE, n = 7–14), respectively. Using Eq. 5 and the measured cell surface-to-volume ratio of 4800 cm^{-1}, osmotic water permeabilities (P_f, in cm/s × 10^{-4}) were: 43 (control), 82 (amphotericin-treated), and 120 (CHIP28-expressing). CHIP28 is a mercurial-sensitive plasma membrane water channel expressed widely in fluid-transporting epithelia and endothelia (Verkman, 1993; Agre et al., 1993).

Curve *f* shows that exposure of the CHIP28-expressing LLC-PK1 cells to $HgCl_2$ (0.3 mM) slows osmotic water transport, giving an exponential time constant of 8.7 ± 0.9 s^{-1} (n = 5) corresponding to a P_f of 49 × 10^{-4} cm/s. This P_f value is similar to that measured in the control (non-transfected) cells above, as well as in various cell types and lipid bilayers not containing water channels (Finkelstein, 1987).

Measurement of water permeability in Sf-9 cells showed no difference between control, WCH-CD-expressing and GLIP-expressing cells. All cell types showed a very rapid fluorescence decay ($\tau \sim 3$ s, data not shown). Since this time constant is near the resolution limit of the instrument, attempts were made to slow the response. As can be seen from Eq. 5, for a given P_f, τ is predicted to increase by lowering the initial cell osmolality, ϕ_o. Experiments conducted at ϕ_o = 200 mOsm increased the time constant for all cell types to 4–5 s ($P_f \sim 0.02$ cm/s). The presence of functional expressed water channels could not be determined with certainty under the conditions of the experiment given the high basal water permeability of the Sf-9 cell plasma membrane.

The measurement of solute permeabilities by TIR fluorescence is shown in Fig. 6. Perfusion of Sf-9 cells with a hypertonic solution to give a 100 mOsm NaCl inwardly directed osmotic gradient resulted in increased TIR fluorescence and a stable plateau; replacement by isosmotic perfusate (PBS) returned the signal to its initial level. The same maneuver performed with a permeant solute, where the excess 100 mOsm NaCl was replaced by an equivalent osmolality of urea or glycerol, produced a similar signal increase, due to osmotic water efflux, followed by a slower decline in

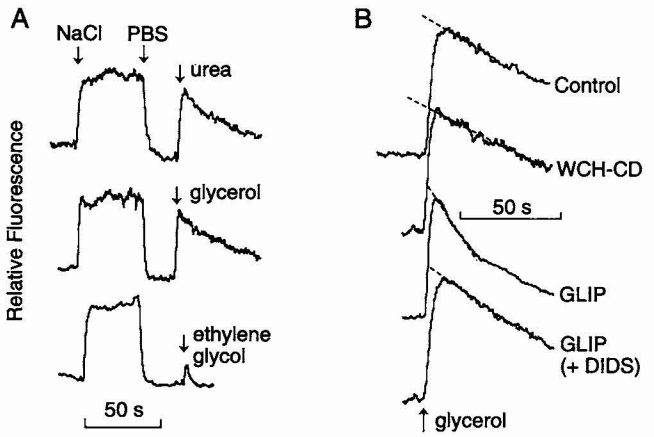

FIGURE 6 Response of Sf-9 cells to 100 mOsm gradients of glycerol and urea at 23°C. (*A*) Wild-type virus-infected Sf-9 cells initially in PBS (300 mOsm) were subjected to a 100 mOsm NaCl gradient, switched back to PBS, and then subjected to 100 mOsm gradients of urea, glycerol, or ethylene glycol. (*B*) Control Sf-9 cells and Sf-9 cells expressing WCH-CD or GLIP proteins were exposed to 100 mOsm glycerol gradients. Where indicated, 0.1 mM DIDS was present in the perfusion solution. See text for averaged solute permeability coefficients.

signal resulting from solute (and water) influx. Using the measured surface-to-volume ratio of 2500 cm^{-1} for Sf-9 cells, Eq. 7 gives urea and glycerol permeabilities of $(4.3 \pm 0.84) \times 10^{-6}$ and $(3.6 \pm 0.44) \times 10^{-6}$ cm/s, respectively. An inward gradient of the highly permeable solute ethylene glycol produced a small fluorescence increase followed by a rapid decrease to the original signal level. From analysis of the coupled solute/water transport described by the Kedem-Katchalsky equation (Chen et al., 1988), the shape of the TIR fluorescence response would provide quantitative information about solute permeability and reflection coefficient.

To test whether GLIP was expressed functionally at the cell plasma membrane, glycerol transport in Sf-9 cells expressing GLIP, a putative glycerol transporting protein, or WCH-CD, a water selective transporting protein was compared to control cells. Cells were exposed to a 100 mOsm glycerol gradient; representative data are shown in Fig. 6 *B*. GLIP-expressing cells had a faster initial rate of fluorescence decrease than did the control (Fig. 6 *B*) or WCH-CD-expressing cells. $P_{glycerol}$ values calculated from Eq. 7 (in cm/s $\times 10^{-6}$) were: 3.6 ± 0.4 (control cells), 5.7 ± 1.4 (WCH-CD-expressing cells), and 13 ± 2 (GLIP-expressing cells). The increased glycerol permeability in the GLIP-expressing cells was partially inhibited (66%) by 100 mM DIDS (4,4′-diisothiocyano-2,2′-disulfonic stilbene). These results indicate that GLIP is functionally expressed at the plasma membrane. Measurement of urea permeability showed no significant difference in P_{urea} for GLIP-expressing [$(8.3 \pm 1.3) \times 10^{-6}$ cm/s] vs. control [$(6.6 \pm 1.4) \times 10^{-6}$ cm/s] cells (data not shown), indicating that GLIP does not function as a urea channel.

DISCUSSION

A simple method was developed to measure continuously the relative volume of living cells immobilized on a transparent substrate for application to studies of plasma membrane permeability and cell volume regulation. Our method utilized total internal reflection (TIR) microfluorimetry to quantify the relative concentration of a fluorescent fluid-phase marker entrapped in the cell cytosol. Because the TIR fluorescence signal was approximately proportional to inverse cell volume, relatively large volume-dependent signals could be measured in real-time for cells of arbitrary shape and size. The TIR fluorescence method has distinct advantages over light scattering (Fischbarg et al., 1989; Echevarria and Verkman, 1992), particle tracking (Kao et al., 1994), and cell shape reconstruction (Strange and Spring, 1987) methods in terms of simplicity, the ability to interpret the optical data quantitatively, and the lack of restrictions on cell geometry. Although the measurement of cytoplasmic fluorophore concentration by confocal microscopy would in principle have similar advantages, the TIR fluorescence method is associated with a considerably smaller effective depth of focus (TIR, 150 nm vs. confocal microscopy, 1000 nm), making TIR measurements relatively insensitive to cell geometry. Furthermore, confocal microscopy requires illumination of the whole cytoplasm, leading to dye photobleaching and extensive baseline correction. In contrast, with TIR illumination only a small fraction of the highly mobile dye in the cell cytoplasm is illuminated so that photobleaching is not a concern.

Control studies (Fig. 2) indicated that the TIR fluorescence signal was insensitive to changes in intracellular and extracellular refractive indices under the conditions of the experiment. The relatively large TIR fluorescence signal amplitudes in response to changes in cell volume eliminated the need for baseline drift corrections. For small changes in cell volume, relative fluorescence was equal to relative osmolality (Fig. 3). This simple relation facilitates the rapid quantitative analysis of data without the need for extensive calibration of the relationship between TIR fluorescence signal and cell volume. The deviations of relative TIR fluorescence versus relative perfusate osmolality from ideality for larger changes in cell volume are probably due to the inability of cells to swell indefinitely without bursting (for relative osmolality <1), and to cell shape changes and/or non-uniform dye distribution (for relative osmolality >1).

The response of the TIR fluorescence signal to changes in cell volume is not instantaneous but depends on the diffusion kinetics of the cytosol-entrapped fluorophore. In bulk cytosol, the diffusion of small fluorophores has been measured by time-resolved anisotropy (Fushimi and Verkman, 1991), photobleaching recovery (Kao et al., 1993) and viscosity-dependence fluorescence (Luby-Phelps et al., 1993) to be very fast (diffusion coefficient > 10^{-6} cm^2/s). Bicknese et al. (1993) showed recently by time-resolved TIR fluorescence anisotropy that cytoplasmic viscosity in membrane-adjacent cytoplasm was similar to that in bulk cytoplasm. The characteristic diffusion time for fluorophore movement across a 100-nm evanescent field depth would thus be ≪1 ms. Therefore, the response time of the TIR fluorescence signal is limited primarily by the fluid exchange rate and instrument response rather than by fluorophore diffusion.

The time course of cell TIR fluorescence in response to solute gradients, together with cell surface-to-volume measurement by confocal image reconstruction, allowed measurement of absolute osmotic water and solute permeability coefficients. Surprisingly, P_f for non-transfected and wild-type virus-infected Sf-9 cells was high (>0.015 cm/s at 10°C), precluding the measurement of small increases in water permeability associated with water channel expression. The high P_f in Sf-9 cells suggests the presence of a water channel in the plasma membrane. In contrast, P_f in non-transfected LLC-PK1 cells was low and similar to that in membranes not containing water channels. The low P_f in LLC-PK1 cells made possible the measurement of an incremental water permeability conferred by membrane insertion of the artificial water channel Amphotericin B and the expression of the erythrocyte/epithelial water channel CHIP28.

The permeability coefficients of uninfected Sf-9 cells for glycerol and urea were comparable to values found in cell plasma membranes and liposomes not containing glycerol/urea transporting proteins. The glycerol permeability coefficients of GLIP-expressing and control cells (Fig. 6) indicated that functional GLIP protein was expressed at the Sf-9 cell plasma membrane. As in *Xenopus* oocytes, the expressed GLIP protein conferred selective stilbene-sensitive glycerol permeability. Urea was not transported measurably by the GLIP protein. The functional expression of GLIP represents the first application of the baculovirus/Sf9 cell system for expression of proteins of the water channel family.

The use of TIR to measure cell volume represents one of the few cellular applications of TIR reported to date. Based on the ability to excite selectively fluorophores very near a glass substrate, TIR has been applied to visualize qualitatively the geometry of surface contact points between the cell membrane and the underlying glass substrate (Axelrod, 1981; Gingell et al., 1985; Reichert and Truskey, 1990; Lanni et al., 1985); a recent report explored the feasibility of multi-angle TIR fluorescence to measure submicroscopic distances (Burmeister et al., 1994). We have been interested in TIR microfluorimetry as a unique approach to examine the rheology and signaling mechanisms in membrane-adjacent cytosol (Bicknese et al., 1993; 1994). Other non-cellular biological applications utilizing TIR polarization and photobleaching recovery have included measurement of ligand affinity and binding kinetics to an immobilized substrate (Axelrod et al., 1986; Pisarchick et al., 1992), and fluorophore orientation and rotational diffusion in thin lipid films (Thompson et al., 1984; Timbs and Thompson 1990; Thompson and Burghardt, 1986).

In Figs. 2, 3, 5, and 6, the total TIR fluorescence signal was measured from ~100 LLC-PK1 or ~300 Sf-9 cells in the field of view. However, a high magnification objective or the use of image detection would allow TIR fluorescence to be collected for single cells (e.g., Fig. 4 *A*) for analysis of samples having heterogeneity in cell composition (e.g., primary cell cultures) and/or function (e.g., transient cDNA transfection, cell cycle variation). The apparatus for measurement of TIR fluorescence utilized a glass prism coupled optically to a glass coverslip to form the high refractive index (glass) to low refractive index (water/cell) interface. Alternative optical configurations for specialized applications are possible. For studies of cell volume in intact tissues in vivo or microdissected in vitro, TIR illumination and detection can be accomplished by a denuded optical fiber coupled to an illumination/detection system by an objective lens and dichroic beam splitter. To modify an existing epifluorescence microscope for TIR fluorescence measurements, the conventional objective can be replaced with an objective of 1.4 numerical aperture in which the back focal plane has been partially blocked to illuminate the sample at supercritical angles (Stout and Axelrod, 1989). Measurement of relative cell volume by TIR can readily be combined with measurements of various cell parameters (e.g., pH, ion activities, membrane potential) utilizing suitable fluorescent indicators and epi-illumination optics. For example, simultaneous measurements of cell volume and cytosolic calcium, and of cell volume and ion activities, have been particularly useful for analysis of signaling and volume regulatory mechanisms in fluid-transporting cells (Foskett, 1990).

We thank Drs. T. Ma and A. Frigeri for constructing the WCH-CD and GLIP pBlueBac III vectors and Dave Hackos for providing Sf-9 cells as well as invaluable guidance in establishing the baculovirus expression system.
This work was supported by grants DK43840 and DK35124 from the National Institutes of Health and a grant from the National Cystic Fibrosis Foundation. J.F. was supported by a graduate student fellowship and V.S. by an undergraduate summer student fellowship from the American Heart Association, California Affiliate. The Achievement Rewards for College Scientists Foundation also provided generous support for J.F.

APPENDIX

The dependence of the TIR fluorescence signal, F, on cell volume, V, is given by:

$$F(V) = \kappa \int\int\int_{Vxyz} I(x, y, z) D(x, y, z)\, dV \qquad (A1)$$

where κ is an instrument constant which depends on the details of the optics and detector, I is the evanescent field intensity, and $D(x,y,z)$ is the dye concentration. For TIR excitation in an homogeneous medium (Hecht, 1987):

$$I(x, y, z) = E_o^2 \exp(-2\beta z) \qquad (A2)$$

$$\beta = (2\pi/\lambda)[\sin^2\theta_i/(n_{aq}/n_g)^2 - 1]^{1/2}$$

where E_o^2 is related to incident beam intensity, λ is wavelength, θ_i is beam incidence angle with respect to the normal, n_{aq} is the refractive index of the aqueous phase, n_g is the refractive index of the glass prism, and β is a measure of the evanescent field penetration depth. For an idealized rectangular cell with dimensions (in dimensionless units) of $1 \times 1 \times V$ ($l \times w \times h$) and assuming that the dye is uniformly distributed in the cell cytoplasm [$D(x, y, z) = D$]:

$$F = \kappa D [1 - \exp(-2\beta V)] \qquad (A3)$$

The dependence of relative fluorescence on osmolality is obtained from Eq. A-3 and an equation relating perfusate osmolality, ϕ, to cell volume. Since the cytosolic dye is membrane impermeable, the product VD is constant. For a perfect osmometer ($V\phi = V_o\phi_o$) with a large cell height-to-probe depth ($\beta V_o \gg 1$) (model *a*):

$$F/F_o = \phi/\phi_o \qquad (A4)$$

For a perfect osmometer with a small height-to-probe depth ($\beta V_o \sim 1$) (model *b*):

$$\frac{F}{F_o} = \frac{(\phi/\phi_o)[1 - \exp(-2\beta V_o \phi/\phi_o)]}{1 - \exp(-2\beta V_o)} \quad \text{(A5)}$$

If a fraction, b/V_o, of cell volume is osmotically inactive [$(V - b)\phi = (V_o - b)\phi_o$] and the cell height-to-probe depth ratio is small (model *c*):

$$\frac{F}{F_o} = \frac{\phi/\phi_o}{1 - b/V_o + (b/V_o)\,\phi/\phi_o} \quad \text{(A6)}$$

The first three models assume that cell shape is invariant as cell volume changes. Model *d* includes cell shape changes by forcing cell volume change to occur at constant cell surface area. Consider an idealized cell geometry consisting of an ellipsoid of revolution, $x^2/\rho^2 + y^2/\rho^2 + (z - c)^2/\sigma^2 = 1$, where ρ and σ are the dimensions of the principal axes in dimensionless units. The values of ρ and σ are calculated as a function of the cell volume, $V = 4/3\pi\rho^2\sigma$ and surface area $= 2\pi\rho^2 + p\sigma^2/\epsilon \ln[(1 + \epsilon)/(1 - \epsilon)]$, where $\epsilon = (1 - \sigma^2/\rho^2)^{1/2}$. As the cell shrinks, it flattens and carries more dye into the evanescent field detection region. Assuming that the cell behaves as a perfect osmometer, it follows that

$$\frac{F}{F_o} = \frac{(\phi/\phi_o)\exp[-2\beta(\sigma - \sigma_o)] \int_0^{\rho} \sinh[2\beta\sigma\sqrt{1 - r^2/\rho^2}]r\,dr}{\int_0^{\rho_o} \sinh[2\beta\sigma_o\sqrt{1 - r^2/\rho_0^2}]r\,dr}$$

where σ_o and ρ_o define initial cell volume and surface area and σ and ρ were calculated by varying the volume while keeping the surface area constant. Eq. A-7 was integrated numerically to generate F/F_o vs. ϕ/ϕ_o curves.

REFERENCES

Agre, P., G. Preston, B. Smith, J. Jung, S. Raina, C. Moon, W. Guggino, and S. Nielsen. 1993. Aquaporin CHIP: the archetypal molecular water channel. *Am. J. Physiol.* 265:F463–476.

Axelrod, D. 1981. Cell-substrate contacts illuminated by total internal reflection fluorescence. *J. Cell Biol.* 89:141–145.

Axelrod, D., R. M. Fulbright, and E. H. Hellen. 1986. Adsorption kinetics on biological membranes: measurement by total internal reflection fluorescence. *In* Applications of Fluorescence in Biomedical Sciences. D. Lansing Taylor, A. S. Waggoner, F. Lanni, R. F. Murphy, and R. R. Birge, editors. Alan R. Liss, Inc., New York. 461–476.

Bicknese, S., J. Farinas, H. P. Kao, and A. S. Verkman. 1994. Novel applications of total internal reflection microfluorimetry in living cells: measurement of cell volume and characterization of membrane-adjacent cytoplasm. *Mol. Biol. Cell* 5:S:249A (Abstr.).

Bicknese, S., N. Periasamy, S. B. Shohet, and A. S. Verkman. 1993. Cytoplasmic viscosity near the cell plasma membrane: measurement by evanescent field frequency-domain microfluorimetry. *Biophys. J.* 65:1272–1282.

Burmeister, J., G. A. Truskey, and W. M. Reichert. 1994. Quantitative analysis of variable-angle total internal reflection fluorescence microscopy (VA-TIRFM) of cell/substrate contacts. *J. Microsc.* 173:39–51.

Chen, P-Y., D. Pearce, and A. S. Verkman. 1988. Membrane water and solute permeability determined quantitatively by self-quenching of an entrapped fluorophore. *Biochemistry.* 27:5713–5719.

Echevarria, M., and A. S. Verkman. 1992. Optical measurement of osmotic water transport in cultured cells: evaluation of the role of glucose transporters. *J. Gen. Physiol.* 99:573–589.

Finkelstein, A. 1987. Water Movement Through Lipid Bilayers, Pores, Plasma Membranes: Theory and Reality. John Wiley and Sons, New York.

Fischbarg, J., K. Kumyar, J. Hirsch, S. Lecuona, L. Rogozinski, S. Silverstein, and J. Loike. 1989. Evidence that the glucose transporter serves as a water channel in J774 macrophages. *Proc. Natl. Acad. Sci. USA.* 86: 8397–8401.

Foskett, J. K. 1990. $[Ca^{2+}]_i$ modulation of Cl^- content controls cell volume in single salivary acinar cells during fluid secretion. *Am. J. Physiol.* 259: C998–1054.

Frigeri, A., M. Gropper, C. W. Turck, and A. S. Verkman. 1995. Immunolocalization of water channel homologs MIWC, and GLIP in epithelial cell plasma membranes. *Proc. Natl. Acad. Sci. USA.* In press.

Fushimi, K., S. Uchida, Y. Hara, Y. Hirata, F. Marumo, and S. Sesaki. 1993. Cloning and expression of apical membrane water channel of rat kidney collecting tubule. *Nature.* 361:549–552.

Fushimi, K., and A. S. Verkman. 1991. Low viscosity in the aqueous domain of cell cytoplasm measured by picosecond polarization microscopy. *J. Cell Biol.* 112:719–725.

Gingell, D., I. Todd, and J. Bailey. 1985. Topography of cell-glass apposition revealed by total internal reflection fluorescence of volume markers. *J. Cell Biol.* 100:1334–1338.

Hecht, E. 1987. Optics. Addison-Wesley Publishing Company, Menlo Park, CA.

Kao, H. P., J. R. Abney, and A. S. Verkman. 1993. Determinants of the translational diffusion of a small solute in cell cytoplasm. *J. Cell Biol.* 120:175–184.

Kao, H. P., and A. S. Verkman. 1994. Tracking of single fluorescent particles in three dimensions: use of cylindrical optics to encode particle position. *Biophys. J.* 67:1291–1300.

Lanni, F., A. S. Waggoner, and D. L. Taylor. 1985. Structural organization of interphase 3T3 fibroblasts studied by total internal reflection fluorescence microscopy. *J. Cell Biol.* 100:1091–1102.

Luby-Phelps, K., S. Mujundar, R. Mujundar, L. Ernst, W. Galbraith, and A. Waggoner. 1993. A novel fluorescence ratiometric method confirms the low solvent viscosity of the cytoplasm. *Biophys. J.* 65:236–242.

Luby-Phelps, K., D. Taylor, and F. Lanni. 1986. Probing the structure of cytoplasm. *J. Cell Biol.* 102:2015–2022.

Ma, T., A. Frigeri, H. Hasegawa, and A. S. Verkman. 1994. Cloning of a water channel homolog expressed in brain meningeal cells and kidney collecting duct that functions as a stilbene-sensitive glycerol transporter. *J. Biol. Chem.* 269:21845–21849.

Montrose-Rafizadeh, C., and W. Guggino. 1990. Cell volume regulation in the nephron. *Annu. Rev. Physiol.* 52:761–772.

Muallem, S., B. Zhang, P. Loessberg, and R. Star. 1992. Simultaneous recording of cell volume changes and intracellular pH on Ca^{2+} concentration in single Osteosarcoma cells UMR-106–01. *J. Biol. Chem.* 267: 17658–17664.

O'Reilly, D., L. Miller, and V. Luckow. 1994. Baculovirus Expression Vectors: A Laboratory Manual. Oxford University Press, New York.

Pisarchick, M., D. Gesty, and N. Thompson. 1992. Binding kinetics of an anti-dinitrophenyl monoclonal Fab on supported phospholipid monolayers measured by total internal reflection with fluorescence photobleaching recovery. *Biophys. J.* 63:215–223.

Reichert, W. M., and G. A. Truskey. 1990. Total internal reflection fluorescence (TIRF) microscopy. I. Modelling cell contact region fluorescence. *J. Cell Sci.* 96:219–230.

Stout, A., and D. Axelrod. 1989. Evanescent field excitation of fluorescence by epi-illumination microscopy. *Appl. Optics.* 28:5237–5242.

Strange, K., and K. A. Spring. 1987. Cell membrane water permeability of rabbit cortical collecting duct. *J. Membr. Biol.* 96:27–43.

Thompson, N. L., and T. P. Burghardt. 1986. Total internal reflection fluorescence: measurement of spatial and orientational distributions of fluorophores near planar dielectric interfaces. *Biophys. Chem.* 25:91–97.

Thompson, N. L., H. M. McConnell, and T. P. Burghardt. 1984. Order in supported phospholipid monolayers detected by the dichroism of fluorescence excited with polarized evanescent illumination. *Biophys. J.* 46:739–747.

Timbs, M. M., and N. L. Thompson. 1990. Slow rotational mobilities of antibodies and lipids associated with substrate-supported phospholipid monolayers as measured by polarized fluorescence photobleaching recovery. *Biophys. J.* 58:413–428.

Van Hoek, A. N., and A. S. Verkman. 1992. Functional reconstitution of the isolated erythrocyte water channel CHIP28. *J. Biol. Chem.* 267:18267–18269.

Verkman, A. S. 1993. Water channels. *In* Molecular Biology Intelligence Series. R. G. Landes Company, Austin, Texas.

Verkman, A. S., W. Lencer, D. Brown, and D. A. Ausiello. 1988. Endosomes from kidney collecting tubule contain the vasopressin-sensitive water channel. *Nature (Lond.).* 333:268–269.